Formation and Dynamics of Antiferromagnetic Correlations in Tunable Optical Lattices

Daniel Greif,[1,2] Gregor Jotzu,[1] Michael Messer,[1] Rémi Desbuquois,[1,*] and Tilman Esslinger[1]
[1]*Institute for Quantum Electronics, ETH Zurich, 8093 Zurich, Switzerland*
[2]*Department of Physics, Harvard University, Cambridge, Massachusetts 02138, USA*
(Received 2 September 2015; published 23 December 2015)

We report on the observation of antiferromagnetic correlations of ultracold fermions in a variety of optical lattice geometries that are well described by the Hubbard model, including dimers, 1D chains, ladders, isolated and coupled honeycomb planes, as well as square and cubic lattices. The dependence of the strength of spin correlations on the specific geometry is experimentally studied by measuring the correlations along different lattice tunneling links, where a redistribution of correlations between the different lattice links is observed. By measuring the correlations in a crossover between distinct geometries, we demonstrate an effective reduction of the dimensionality for our atom numbers and temperatures. We also investigate the formation and redistribution time of spin correlations by dynamically changing the lattice geometry and studying the time evolution of the system. Time scales ranging from a sudden quench of the lattice geometry to an adiabatic evolution are probed.

DOI: 10.1103/PhysRevLett.115.260401 PACS numbers: 05.30.Fk, 37.10.Jk, 67.85.Lm, 75.78.-n

Understanding the mechanisms underlying quantum magnetism is among the most thought-provoking challenges of quantum many-body physics. At the center of these efforts is the interplay between the emergence of magnetic correlations and the underlying lattice geometry [1]. Extensive research has been carried out using different materials, as well as theoretical and numerical methods, which enhanced the understanding and also triggered unforeseen questions [2,3]. A new development is the study of quantum magnetism using ultracold fermionic atoms in optical lattices. In these systems, magnetic ordering arises from a quantum-mechanical exchange coupling between the constituent atoms with different spins. This approach offers a uniquely direct link between experimental observations and theoretical models, a key element for quantum simulation [4,5]. It also promises unprecedented dynamic control over lattice parameters and geometry [6–10], which can give an entirely new perspective on out-of-equilibrium properties of quantum spin systems [11]. Indeed, antiferromagnetic spin correlations were recently observed in the Hubbard regime of an optical lattice, first in an anisotropic [12] and later in an isotropic simple cubic geometry [13]. In both situations, highly sophisticated computational methods were required for comparison between experiment and theory [13–16]. Along a different line, making use of ultracold bosons, progress was made in simulating static and dynamic properties of classical and quantum mechanical spin models in theoretically more tractable regimes [17–23].

In this Letter, we explore the emergence of antiferromagnetic spin correlations in different lattice geometries of varying dimensionality, also including crossover configurations between different geometries. The dynamic control over the geometries enables us to study the formation dynamics and the redistribution time of spin correlations, where the explored time scales range from the sudden to the adiabatic regime. The starting point of the experiment is a harmonically confined ultracold Fermi gas of ^{40}K in a balanced two-component spin mixture with repulsive interactions [12]. The atoms are prepared in the two magnetic sublevels $m_F = -9/2$, $-7/2$ of the $F = 9/2$ hyperfine manifold, and the s-wave scattering length is tuned between $136.4(5) - 149.0(3)a_0$ via the Feshbach resonance located at 202.1 G (a_0 denotes the Bohr radius). For all experiments, the atom number is $140(30) \times 10^3$ with 10% systematic error, and the temperature is $0.09(1)T_F$, where T_F is the Fermi temperature. After the preparation, the atoms are loaded into the lowest band of a tunable-geometry optical lattice using an S-shaped ramp lasting 100 ms. This ramp is nearly adiabatic, and the entropy it creates does not significantly depend on the chosen geometry [24]. The lattice consists of several retroreflected interfering and noninterfering laser beams of wavelength $\lambda = 1064$ nm, which gives access to a broad variety of lattice geometries [8,24]. Additionally, in all measurements, a 3D harmonic confinement is present in the experiment with a geometric mean trapping frequency of $\bar{\omega}/2\pi = 57(1)$ Hz. This causes a locally varying lattice filling over the size of the cloud, with its largest value in the center of the trap.

Our experiments are well described by the Fermi-Hubbard Hamiltonian

$$\hat{H} = -\sum_{\langle ij\rangle,\sigma} t_{ij}(\hat{c}^{\dagger}_{i\sigma}\hat{c}_{j\sigma} + \text{H.c.}) + U\sum_i \hat{n}_{i\uparrow}\hat{n}_{i\downarrow} + \sum_{i,\sigma} V_i \hat{n}_{i\sigma}, \quad (1)$$

with tunneling t_{ij} between nearest neighbors $\langle ij \rangle$ and repulsive on-site interaction U. Here, $\hat{c}^{\dagger}_{i\sigma}$ and $\hat{c}_{i\sigma}$ denote the fermionic creation and annihilation operators for the two spin states $\sigma \in \{\uparrow, \downarrow\}$, the density operator is denoted by $\hat{n}_{i\sigma} = \hat{c}^{\dagger}_{i\sigma}\hat{c}_{i\sigma}$ and V_i is the trap energy. The different lattice geometries are realized experimentally by independently adjusting the specific values of t_{ij} for each of the six nearest neighbor links per lattice site of an underlying simple cubic lattice. Their strength is controlled via the power of the lattice laser beams [24]. In all measurements presented in the following, we adjust the scattering length with a Feshbach resonance such that $U/h = 0.87(2)$ kHz and set the total bandwidth for noninteracting particles to $W/h = 2.6(1)$ kHz [27].

After loading the atoms into the desired lattice geometry, we measure the trap-averaged magnetic spin correlations emerging on neighboring sites in the low-temperature many-body state of the quantum gas. Our detection is similar to the method used in previous experiments [12] and is presented in full detail in the Supplemental Material [24]. The spin correlations are measured on every second lattice link, between nearest neighbors i and $i+1$, and along the transverse spin axis

$$C_{i,i+1} = -\langle \hat{S}^x_i \hat{S}^x_{i+1} \rangle - \langle \hat{S}^y_i \hat{S}^y_{i+1} \rangle. \quad (2)$$

Here, $\hat{S}^{x,y,z}_i$ denote the standard spin vector operators for a spin-1/2 system on site i, and $\langle \ldots \rangle$ denotes the trap average. For SU(2) symmetry, $C_{i,i+1}$ is equal to $-2\langle \hat{S}^z_i \hat{S}^z_{i+1} \rangle$. The detection protocol allows us to measure both antiferromagnetic and ferromagnetic configurations, corresponding to positive and negative values of $C_{i,i+1}$, respectively.

In a first measurement, we investigate the strength of spin correlations in several different lattice geometries. Starting from an underlying simple cubic lattice, the tunneling is enhanced along Z nearest neighbor links and takes the value t_s, whereas the tunneling along the remaining $6 - Z$ links is $t_s/5$. The geometries realized in this manner are, sorted by increasing number of strong nearest neighbor links Z: dimerized, 1D chains, honeycomb (HC) planes, ladders, square, coupled honeycomb planes, and cubic (see Fig. 1). We measure the correlations along the strong tunneling links. As shown in Fig. 1, the strength of the correlations depends on the specific geometry with values ranging between 0.084(1) and 0.010(1) for the trap averaged value, and is generally smaller for a larger number of strong tunneling links. In the isotropic cubic lattice as well, which has the largest value of Z ($Z = 6$), we detect antiferromagnetic correlations in the system [13].

The observed dependence of the spin correlator on Z can be understood with two simple arguments in a homogeneous system. Owing to the isolated nature of the system, the total entropy rather than the temperature is constant for different Z. First, with a finite entropy, the presence of two

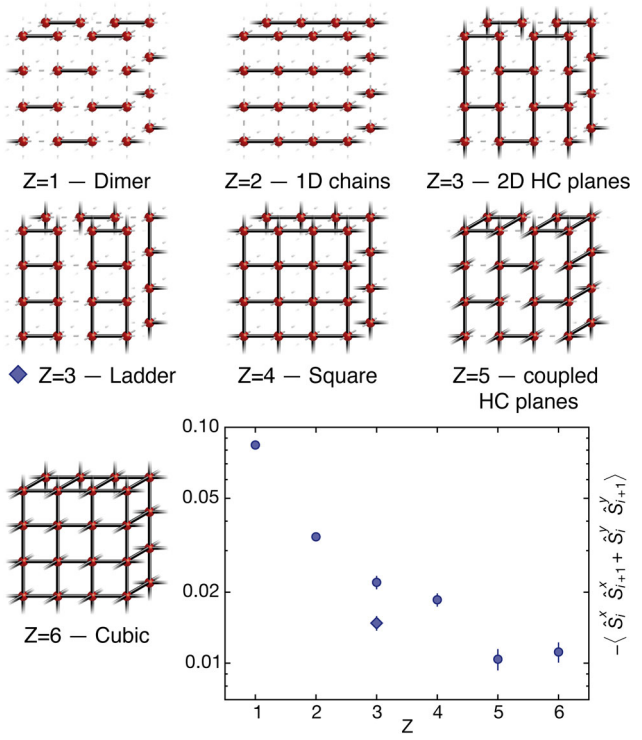

FIG. 1 (color online). Experimental observation of the dependence of antiferromagnetic correlations on lattice geometry. The trap averaged correlator $-\langle \hat{S}^x_i \hat{S}^x_{i+1} \rangle - \langle \hat{S}^y_i \hat{S}^y_{i+1} \rangle$ is measured along the strong links for various lattice geometries, which differ in the number of strong nearest neighbor links Z. Additionally, a schematic view of the lattice geometries is shown, where the strong tunneling links are indicated by a bar. For all data points, the bandwidth $W/h = 2.6(1)$ kHz and the on-site interaction $U/h = 0.87(2)$ kHz is constant. Error bars denote the standard error of 50 measurements.

different energy scales associated with different tunnelings directly affects the magnetic correlations and leads to a redistribution of spin correlations between the strong and the weak links. For a large number of weaker tunneling links, more low-energy states are accessible. Thus, a finite entropy mainly leads to thermal fluctuations within these states, and the magnetic correlator on the strong links is high. However, if the number of weak links decreases, thermal fluctuations along the weak links alone are not sufficient to account for the total entropy, and additional thermal fluctuations are also distributed on the strong links, therefore, reducing the strong link correlator. Second, even at zero entropy, quantum fluctuations play a significant role. In lower dimensions, this generally leads to enhanced short-range spin correlations [29]. In both cases, the correlator is expected to decrease as Z is increased. This is in accordance with previous measurements in the specific cases of dimerized lattices ($Z = 1$) and 1D chains ($Z = 2$) [12,15].

While these two effects predict a dependence only on Z, the lattice geometry itself (for the same value of Z) will also affect the strength of the spin correlations, most importantly

at low temperatures. In fact, in the limit of vanishing temperatures, the state of the system and its phase diagram will be entirely determined by the interplay between geometry and magnetic ordering. The different values observed for the two $Z = 3$ geometries (ladder and honeycomb planes) might be due to a higher entropy in the ladder geometry [24], or it could suggest that effects of the lattice geometry are already starting to play a role at the temperatures reached in the experiment. An analysis of the relative importance of these effects may be achieved by a detailed experiment-theory comparison, which is beyond the scope of this Letter.

In addition to the aforementioned contributions, the underlying harmonic confinement also plays a central role for the value of the trap-averaged correlator. Within the local density approximation, both the chemical potential at the center of the trap and the temperature are determined by the total atom number and entropy. As the equation of state of the system depends on the lattice geometry and Z, both the density and entropy distribution change with the geometry, which directly affects the magnetic correlator.

To further study the impact of geometry on magnetic correlations, we measure their strength for a crossover regime between two lattice geometries with different numbers of strong links Z. In the experiment, geometries with a different Z can be smoothly connected by adjusting the strength of the individual tunneling links [24]. We scan between a square ($Z = 4$) and 1D chain ($Z = 2$) geometry by choosing the strong-to-weak tunneling ratio t_s/t in the range 1–5, while keeping the tunneling in the orthogonal direction at $t_s/5$, see Fig. 2(a). A second scan between a 1D chain and dimerized ($Z = 1$) geometry is shown in Fig. 2(b). We measure spin correlations either along the strong or the weak tunneling links. In both cases, correlations on each link start from the same value. As t_s/t is increased, the correlations along the strong links are enhanced, whereas the correlations along the weak links decrease. Interestingly, the correlations change more rapidly with increasing t_s/t for the scan in Fig. 2(a) as compared to Fig. 2(b), which is a consequence of the underlying lattice geometry. For the final configuration $t_s/t = 5$, the correlations on the weak link have nearly vanished, whereas the correlations on the strong links have saturated at a high value. This indicates that the thermal fluctuations occur predominantly on the weak links. Consequently, the weaker couplings can be neglected in this case, and the dimensionality of the lattice is effectively reduced for our total entropy and atom number. Interestingly, the reduction of the dimensionality occurs at different ratios of t_s/t, depending on which geometry is considered.

These measurements demonstrate that spin correlations redistribute between the strong and weak links when changing Z. Yet, this does not necessarily imply that the sum of spin correlations is constant. We find the sum of correlations to be approximately constant in the scan of Fig. 2(a), whereas it increases significantly with

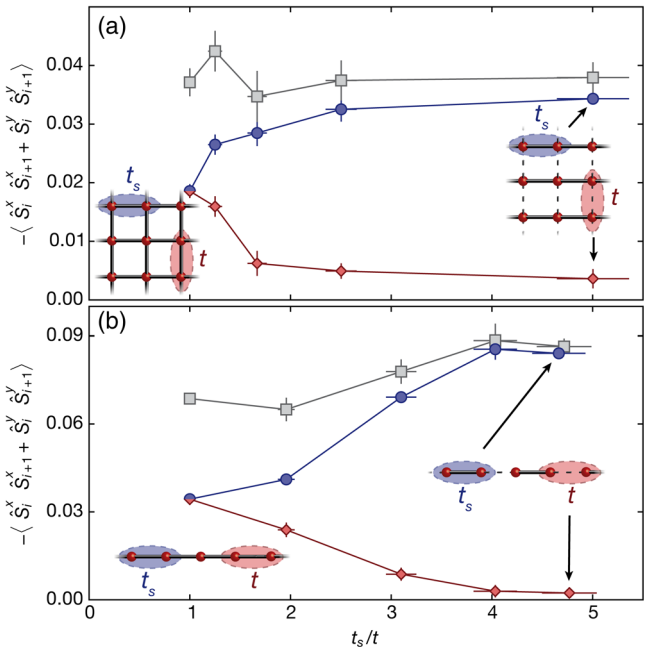

FIG. 2 (color online). Spin correlations for a crossover between two different lattice geometries. (a) Scan between a square ($Z = 4$) and a 1D chain ($Z = 2$) geometry and (b) scan between a 1D chain ($Z = 2$) and a dimerized ($Z = 1$) geometry. In both cases, the strong to weak tunneling ratio t_s/t varies between 1 and 5. Blue and red symbols denote the measured spin correlations along the strong and weak links, respectively. Gray symbols show their sum. The error bar on the tunneling ratio denotes the uncertainty on the lattice parameters, while the data are the mean $\pm$ the standard error of at least 25 measurements.

dimerization in the scan of Fig. 2(b). This observation might be related to the opening of a finite energy gap in the energy spectrum for a strongly dimerized lattice, which causes entropy redistribution within the trapped system and enhances the overall spin correlation strength [12].

The tunability of our lattice also allows us to experimentally measure the time scales for the formation and redistribution of spin correlations when dynamically changing the lattice geometry. This is done by measuring the strength of spin correlations when the lattice geometry is changed on variable time scales. For simplicity, we start with a ramp where the initial and final lattice geometry are the same up to a rotation: starting from a 1D chain geometry we ramp via a square lattice to a 1D chain lattice again, but with strong tunneling along the perpendicular direction. We always include an additional wait time before the ramp such that the total time in the optical lattice is constant, see Fig. 3(a). The spin correlations are measured immediately after the ramp along the two different directions.

The observed dependence of the spin correlations on the total ramp time τ is shown in Fig. 3(a). For fast ramps, $\tau < 1$ ms, the spin correlations remain unchanged at the values without ramping. Here, a nonequilibrium state is

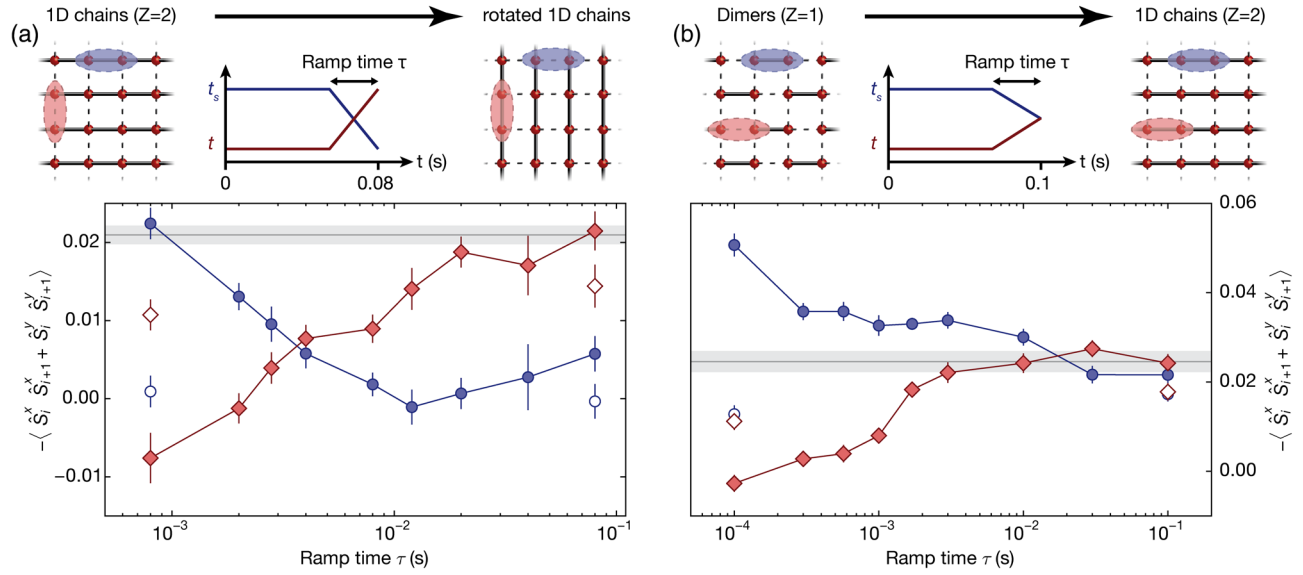

FIG. 3 (color online). Dynamics of spin correlations. The lattice is ramped within a time τ (a) from a 1D chain geometry to the same 1D chain geometry rotated by 90° and (b) from a dimerized to 1D chain geometry [24]. Blue and red points denote the measured spin correlations along the previously and new strong links. For all closed symbols, the correlations are measured immediately after the ramp, whereas open symbols include an additional wait time of 50 ms. The gray solid lines indicate the reference value for the correlations in the initial geometry without the lattice ramp, and the shading denotes the error on this value. Error bars are the standard error of at least 25 measurements.

formed with several charge and spin excitations, which decay when allowing for an additional wait time after the ramp, thus, changing the detected value of spin correlations [open symbols in plot Fig. 3(a)]. On intermediate ramp times, $\tau \sim 4$ ms, the spin correlations change symmetrically along the two directions. This time scale is comparable to the underlying tunneling time between $h/t_s = 2$ ms and $h/t = 10$ ms during the ramp. For very slow ramp times, we observe, within error bars, a 100% transfer of spin correlations from the previously strong to the new strong links. When waiting 100 ms in this case, the magnetic correlations decrease (most likely due to underlying heating of the gas) but agree with the value when loading directly from the harmonic trap to the final lattice geometry and waiting for the same total time. These observations are in agreement with a fully adiabatic ramp to an equilibrated final state for the slowest ramp times, as the initial and final lattice geometries are the same with the same density and entropy distributions.

The situation changes considerably for a ramp with different initial and final lattice geometries. Here, we start from a dimerized lattice with a ratio of $t_s/t = 5$ for adjacent tunneling links and ramp to a 1D geometry without dimerization. Immediately after the lattice ramp, we measure the spin correlations on the initially strong and weak links along the 1D direction, see Fig. 3(b). As before, for fast ramps, the spin correlations cannot redistribute and are nearly unchanged as compared to the case without a ramp. When adding an additional wait time after the fastest ramp, the spin correlations change, signaling a decay of the created excitations in this case. The behavior is different for intermediate ramp times: while the correlations on the initially strong links decrease very quickly, slower ramp times $\tau \sim 1$ ms are necessary for the correlations on the initially weak links to change. This may originate from the difference in the overall tunneling time scale during the ramp for the two links. For the slowest ramps, the correlators along the original strong and weak link are identical. With an additional wait time, they both decay to the same value, again owing to heating. This indicates a final state close to equilibrium. In contrast to the previous measurement, the gap between the ground and excited states closes during the ramp, since the singlet-triplet gap has vanished in the nondimerized geometry. Yet, the observed spin correlation value agrees with a reference when loading directly into the final lattice geometry and holding the remaining time. Consequently, ramp times corresponding to a few tunneling times are already sufficient to reach equilibrium.

In conclusion, we have observed antiferromagnetic correlations in a variety of lattice geometries and studied the redistribution of correlations between strong and weak links. Extending our work to lower temperatures will allow addressing open questions on the low-temperature phase diagram of the Hubbard model in complex lattice geometries. In this way, the nature of the ground state in a spin ladder geometry with tunable couplings can be investigated [2]. It may also be possible to study quantum criticality in the vicinity of the phase transition from a semimetal to an antiferromagnetic Mott insulator in the 2D honeycomb

lattice [30]. In combination with recent efforts on creating spin-dependent optical lattices with very low underlying heating [31], the anisotropic XXZ Heisenberg model and the Falikov-Kimball model could be realized and studied experimentally with ultracold fermions [32]. Our results on quantum spin dynamics demonstrate that ultracold fermions in optical lattices are well suited to study open questions in out-of-equilibrium many-body spin systems, where theoretical methods become extraordinarily difficult [33,34]. Furthermore, the observed rapid formation time scales of spin correlations offer very promising perspectives for the implementation of sophisticated entropy redistribution schemes based on trap shaping and dynamically changing lattice geometries, which are expected to result in overall lower temperatures [35–37].

We would like to thank Frederik Görg, Lei Wang, and Jakub Imriška for insightful discussions and valuable contributions. We acknowledge SNF, NCCR-QSIT, QUIC (Swiss State Secretary for Education, Research and Innovation Contract No. 15.0019) and SQMS (ERC advanced grant) for funding. R. D. acknowledges support from the ETH Zurich Postodoctoral Program and the Marie Curie Actions for People COFUND program.

*desbuquois@phys.ethz.ch

[1] A. Auerbach, *Interacting Electrons and Quantum Magnetism* (Springer, New York, 1994).
[2] T. Giamarchi, *Quantum Physics in One Dimension* (Clarendon Press, Oxford, 2003).
[3] L. Balents, Nature (London) **464**, 199 (2010).
[4] I. Bloch, J. Dalibard, and W. Zwerger, Rev. Mod. Phys. **80**, 885 (2008).
[5] T. Esslinger, Annu. Rev. Condens. Matter Phys. **1**, 129 (2010).
[6] J. Sebby-Strabley, M. Anderlini, P. S. Jessen, and J. V. Porto, Phys. Rev. A **73**, 033605 (2006).
[7] P. Soltan-Panahi, J. Struck, P. Hauke, A. Bick, W. Plenkers, G. Meineke, C. Becker, P. Windpassinger, M. Lewenstein, and K. Sengstock, Nat. Phys. **7**, 434 (2011).
[8] L. Tarruell, D. Greif, T. Uehlinger, G. Jotzu, and T. Esslinger, Nature (London) **483**, 302 (2012).
[9] G.-B. Jo, J. Guzman, C. K. Thomas, P. Hosur, A. Vishwanath, and D. M. Stamper-Kurn, Phys. Rev. Lett. **108**, 045305 (2012).
[10] S. Taie, H. Ozawa, T. Ichinose, T. Nishio, S. Nakajima, and Y. Takahashi, Sci. Adv. **1**, e1500854 (2015).
[11] B. Yan, S. A. Moses, B. Gadway, J. P. Covey, K. R. A. Hazzard, A. M. Rey, D. S. Jin, and J. Ye, Nature (London) **501**, 521 (2013).
[12] D. Greif, T. Uehlinger, G. Jotzu, L. Tarruell, and T. Esslinger, Science **340**, 1307 (2013).
[13] R. A. Hart, P. M. Duarte, T.-L. Yang, X. Liu, T. Paiva, E. Khatami, R. T. Scalettar, N. Trivedi, D. A. Huse, and R. G. Hulet, Nature (London) **519**, 211 (2015).
[14] B. Sciolla, A. Tokuno, S. Uchino, P. Barmettler, T. Giamarchi, and C. Kollath, Phys. Rev. A **88**, 063629 (2013).
[15] J. Imriška, M. Iazzi, L. Wang, E. Gull, D. Greif, T. Uehlinger, G. Jotzu, L. Tarruell, T. Esslinger, and M. Troyer, Phys. Rev. Lett. **112**, 115301 (2014).
[16] A. Golubeva, A. Sotnikov, and W. Hofstetter, Phys. Rev. A **92**, 043623 (2015).
[17] J. Simon, W. S. Bakr, R. Ma, M. E. Tai, P. M. Preiss, and M. Greiner, Nature (London) **472**, 307 (2011).
[18] J. Struck, C. Ölschläger, R. L. Targat, P. Soltan-Panahi, A. Eckardt, M. Lewenstein, P. Windpassinger, and K. Sengstock, Science **333**, 996 (2011).
[19] J. Struck, M. Weinberg, C. Ölschläger, P. Windpassinger, J. Simonet, K. Sengstock, R. Höppner, P. Hauke, A. Eckardt, M. Lewenstein, and L. Mathey, Nat. Phys. **9**, 738 (2013).
[20] T. Fukuhara, P. Schauß, M. Endres, S. Hild, M. Cheneau, I. Bloch, and C. Gross, Nature (London) **502**, 76 (2013).
[21] T. Fukuhara, A. Kantian, M. Endres, M. Cheneau, P. Schauß, S. Hild, D. Bellem, U. Schollwöck, T. Giamarchi, C. Gross, I. Bloch, and S. Kuhr, Nat. Phys. **9**, 235 (2013).
[22] S. Hild, T. Fukuhara, P. Schauß, J. Zeiher, M. Knap, E. Demler, I. Bloch, and C. Gross, Phys. Rev. Lett. **113**, 147205 (2014).
[23] R. C. Brown, R. Wyllie, S. B. Koller, E. A. Goldschmidt, M. Foss-Feig, and J. V. Porto, Science **348**, 540 (2015).
[24] See Supplemental Material at http://link.aps.org/supplemental/10.1103/PhysRevLett.115.260401 for details, which includes Refs. [25,26].
[25] R. Joerdens, N. Strohmaier, K. Guenther, H. Moritz, and T. Esslinger, Nature (London) **455**, 204 (2008).
[26] V. W. Scarola, L. Pollet, J. Oitmaa, and M. Troyer, Phys. Rev. Lett. **102**, 135302 (2009).
[27] All Hubbard parameters are calculated from the lattice potential using Wannier functions, which are obtained using band-projected position operators [28].
[28] T. Uehlinger, G. Jotzu, M. Messer, D. Greif, W. Hofstetter, U. Bissbort, and T. Esslinger, Phys. Rev. Lett. **111**, 185307 (2013).
[29] E. V. Gorelik, D. Rost, T. Paiva, R. Scalettar, A. Klümper, and N. Blümer, Phys. Rev. A **85**, 061602 (2012).
[30] S. Sorella, Y. Otsuka, and S. Yunoki, Sci. Rep. **2**, 992 (2012).
[31] G. Jotzu, M. Messer, F. Görg, D. Greif, R. Desbuquois, and T. Esslinger, Phys. Rev. Lett. **115**, 073002 (2015).
[32] J. K. Freericks and V. Zlatić, Rev. Mod. Phys. **75**, 1333 (2003).
[33] A. Polkovnikov, K. Sengupta, A. Silva, and M. Vengalattore, Rev. Mod. Phys. **83**, 863 (2011).
[34] J. Eisert, M. Friesdorf, and C. Gogolin, Nat. Phys. **11**, 124 (2015).
[35] T.-L. Ho and Q. Zhou, arXiv:0911.5506.
[36] J.-S. Bernier, C. Kollath, A. Georges, L. De Leo, F. Gerbier, C. Salomon, and M. Köhl, Phys. Rev. A **79**, 061601 (2009).
[37] M. Lubasch, V. Murg, U. Schneider, J. I. Cirac, and M.-C. Bañuls, Phys. Rev. Lett. **107**, 165301 (2011).